Materials Science and Engineering B 307 (2024) 117491

Contents lists available at ScienceDirect

Materials Science & Engineering B

journal homepage: www.elsevier.com/locate/mseb

High temperature synthesis and material properties of boron-enriched balk pyrolytic carbon

Marina Demidenko [a], Dzmitry Adamchuk [a], Alexander Liubimau [a,e], Vladimir Uglov [b], Arcady Ishchenko [c], Mikalai Chekan [d], Mikhail Khama [d], Sergey Maksimenko [a,*]

[a] Institute for Nuclear Problems, Belarusian State University, 11 Bobruiskaya str., 220006 Minsk, Belarus
[b] Belarusian State University, Physics Faculty, Nezalezhnasti av. 6, 220006 Minsk, Belarus
[c] Boreskov Institute of Catalysis SB RAS & Novosibirsk State University, Lavrentyev Prospekt 5, Novosibirsk 630090, Russia
[d] Physical Technical Institute of NAS of Belarus, 10 Academician Kuprevich str., 220084 Minsk, Belarus
[e] Belarusian State Technological University, Sverdlova str.13a, Minsk 220006, Belarus

ARTICLE INFO

Keywords:
Pyrolytic carbon
Boron-enriched carbon
Chemical vapor deposition
Friction coefficient
Thermogravimetric analysis
Superhard materials

ABSTRACT

In this paper we report the synthesis and characterization of the boron-enriched pyrolytic carbon (B-PyC). In the research we aimed to propose a material demonstrating high strength characteristics and heat resistance, durability, chemical inertness and biocompatibility. The material has been synthesized by high temperature low pressure CVD method. The synthesis is carried out on the inner surface of a vertically oriented hollow graphite hexagonal prism heated to the temperatures 1450–1570 °C. Controlled low-density flows of nitrogen, boron trichloride and carbonaceous gas react in this zone producing B-PyC film deposited on the vertical graphite plates. Morphology, mechanical and physical properties of this material was investigated using X-ray diffraction, scanning and transmission electron microscopy, mechanical testing instrumentations, thermogravimetric and thermal analysis. It was found that during the synthesis a two-phase crystalline system is organized comprising fragments of graphene layers (pyrolytic carbon) and boron carbide B_4C. Such a structure provides high mechanical properties of the material and their stability in a wide temperature range, heat resistance, chemical inertia and biocompatibility. Depending on the synthesis conditions, the micro hardness may vary in a wide range including the range 100–140 HV the most attractive for traumatology and cardiac surgery as well as for a variety of engineering applications.

1. Introduction

The family of carbon materials is distinguished by a variety of forms and, as a result, physicochemical properties: diamond, graphite, pyrolytic carbon (PyC), carbon fibers, soot, various nanoscale structures such as fullerenes, graphene, carbon nanotubes, onion-like carbon, etc. This diversity also determines the richness of engineering applications in various industries, ranging from traditional electrical engineering to modern wireless communication systems, biomedicine and the industry of advanced technological materials. In particular, in medical technologies, an urgent problem is the development of materials that combine high hardness, durability and long-term performance with biocompatibility and bioinertness, and at the same time allow, to a certain extent at least, shaping and machining. Such requirements are met by an extensive subfamily of pyrolytic carbons. Pyrolytic carbon is a material constituted by arbitrarily oriented fragments of graphene sheets, but with some covalent bonding between these sheets as a result of imperfections of synthesis. Pyrolytic carbon began to be used more than 50 years ago (see e.g. [1]), first in the nuclear industry, and then found wide application in medicine [2,3], electrical engineering and electrochemistry as electrodes and sensing elements [4,5].

Under certain conditions, interlayer bonds in graphite can be significantly enhanced by doping it with atoms of other elements, which can change the distribution of electrons in graphite planes and improve the physicochemical characteristics of the material. From this point of view, one of the promising chemical elements is boron, which is adjacent to carbon in the periodic table of elements and, therefore, has a similar atomic size. The theoretical substantiation of such a variant of solving the problem is presented in [6], where the calculated values of the mechanical characteristics of various boron–carbon compounds are

* Corresponding author.
E-mail addresses: lubimov@belstu.by (A. Liubimau), uglov@bsu.by (V. Uglov), chekan@phti.by (M. Chekan), sergey.maksimenko@gmail.com (S. Maksimenko).

https://doi.org/10.1016/j.mseb.2024.117491
Received 23 April 2024; Received in revised form 27 May 2024; Accepted 3 June 2024
Available online 7 June 2024

given. Starting with pioneering works made in sixtieth [7,8] boron doped pyrolytic carbon materials B_xC_{1-x} ($0 < x < 0.25$) has been widely studied afterward both experimentally [9–14] and theoretically, by numerical simulation of the electronic structure [15–17]. It has been shown that boron is an effective dopant for improving the resistance of a material to oxidation [18,19] and ablation [20] and improving the mechanical properties of materials [21,22]. As it has been discussed in details in Ref. [23], there are several B-C bonding mechanisms in the B-PyC deposition process and the main bonding state of boron element is the substitution of carbon by boron in the graphene lattice [24]. As a result, the formation of single-crystal inclusions of boron carbide B_4C takes place providing advanced properties mentioned above.

One of the main areas of application of boron doped pyrolytic carbon is the medical industry [2,25], and, in particular, cardiac surgery. The fine-grained structure of the material makes it possible to obtain polished surfaces of a high purity class and admissible microhardness. Also, advanced physical chemical properties of the material appear to be attractive for different engineering applications such as perfect sealing in aggregates operating in chemically aggressive or unstable environments, or requiring precise mechanical processing. Promising directions for the introduction of this material are the manufacture of electrodes for supercapacitors [26], sensors, etc. Based on the synthesis procedure developed in our team, in the given paper we report detail investigation of the boron-enriched material demonstrating high strength characteristics and heat resistance, durability, chemical inertness and biocompatibility. In spite of variety of publications on the subject, the analysis performed made it possible to reveal the properties potentially contributing to novel areas of applications, such as wireless communication and aerospace industry.

2. Materials and methods

2.1. Synthesis procedure

Pyrolytic carbon, as a rule, is obtained by the method of chemical vapor deposition (CVD) in reactors on heated, catalytically inactive surfaces during the thermal decomposition of a carbon-containing gas mixture. In the need of boron doping, boron-containing gases are added to the gas mixture. Boron, released during thermal degradation, acts as a catalyst and promotes the formation of dispersed soot particles on a solid graphite substrate, which serve as crystallization centers for the subsequent growth on the top of hexagonal carbon networks [1,27]. The addition of boron chloride to the gas mixture has a significant effect on the growth of PyC phase. Some boron atoms can replace carbon atoms in the hexagonal graphene lattices [28]. An excess of boron that appears in the graphene layers during synthesis can lead to the destruction of hexagonal networks and appearance of various defects in them [29] including formation of boron carbide B_4C. Namely boron carbide provides extraordinal microhardness index of B-PyC which significantly improves the mechanical properties and oxidation resistance of this material.

In general, composition and structure of the boron–carbon composite material is controlled by the gas flow rate, the type of hydrocarbons involved in the synthesis, the temperature, and the surface area of the substrate. To obtain boron enriched pyrolytic carbon, we have developed a CVD setup [30], in which the synthesis of the material was carried out on the inner surface of an indirectly heated hollow graphite hexagonal prism. The prism face is a 30 mm × 120 mm parallelogram. The synthesis time depends on the required thickness. The duration of the synthesis of the samples described in the article, reaching a thickness of 3 mm, was 6 h. To ensure the homogeneity of the synthesized material, the axis of the graphite assembly is oriented vertically. In this case, the agglomerates formed in the hot gas flow fall to the bottom of the coarse filter. High-purity methane (99.999 %), technical propane-butane mixture, high-purity nitrogen (99.999 %) were used as carbon-containing gas. The source of boron is gaseous high purity boron trichloride (99.9999 %). The addition of a propane-butane mixture to the synthesis leads to a significant acceleration of the growth of the material due to the presence of a larger number of carbon atoms in a given volume. Ratio of input gases $N_2/CH_4/C_3H_8/BCl_3$ in the process was as follows: 1/0.7/0.07/0.17. The pressure in the reactor was set in the range of 900–1300 Pa (such a low absolute pressure of carbonaceous gas is used for excessive soot formation). We have found that at a pressure of less than 500 Pa, the growth rate of the material is significantly reduced, while a pressure above 2000 Pa leads to a significant decrease in mechanical characteristics. The ration of gases in mixture and the mixture pressure in the reactor chamber were fixed during the synthesis. Note that, in contrast to role of the temperature and gas mixture velocity, the pressure variation within the above stated range does not significantly affect the structure of the material: Within this range the gas flow provides sufficient energy to proceed the decomposition reactions of hydrocarbon and boron trichloride. The gas flow rate control is implemented by gas flow regulators, as well as a throttle valve at the vacuum pump inlet, which can reduce the capacity of the vacuum line and reduce the rate of pumping out gaseous reaction products (approximately on the level of 8 l/min). It should be noted that a large amount of hydrogen is formed during the synthesis, which prevents the precipitation of layers of pyrolytic carbon with a high degree of order from the gas phase. For pumping out hydrogen, it is possible to purge nitrogen into the pumping line. Fig. 1 shows a schematics of the synthesis setup. Pressure sensors measure the residual pressure in and out of the reactor.

As was mentioned above, one of the main technological parameters of synthesis is deposition temperature, which was in our facility as large as 1570 °C. The substrate temperature was measured indirectly: the pyrometer measures the temperature of a graphite heater, inside which an assembly of graphite substrates is installed, through a quartz window in the metal casing of the reactor. Note that deposition temperature in the reactor exceeds the commonly used temperature conditions (for example, 1550 °C [32], 1250 °C [12], 1173–1373 °C [23], 800 °C [14], 350 °C [13]). Our choice of temperature and pressure in the chamber was dictated by the requirements for the installation in terms of productivity and for the material in terms of microhardness, and was selected experimentally during the work.

After automatic fixation of the synthesis temperature, the gas flow rate is set based on the zone of preferred material disembarkation. Increasing the speed leads to “stretching” of the material over the heated surface. However, with an excessive increase in the gas flow rate in the coarse filter installed before the pump, a large amount of fine boron-graphite dust is formed. This effect is due to the fact that under

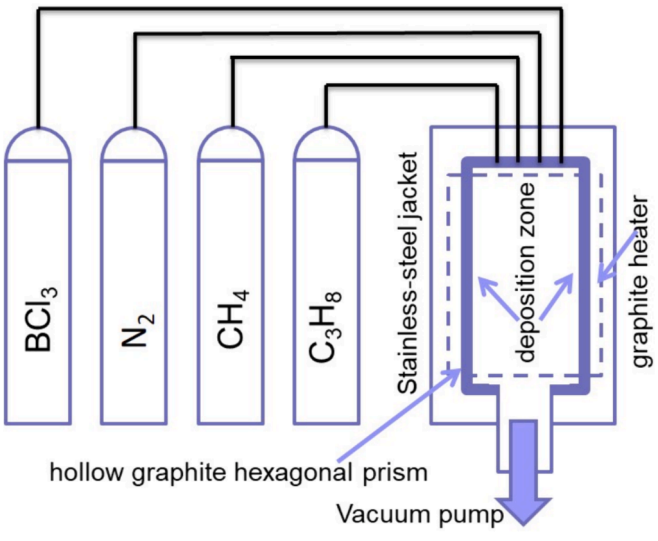

Fig. 1. Schematics of the low pressure CVD set-up.

conditions of high velocity, the gas flow does not have time to heat up and react in the reactor chamber. It has been experimentally established that the energy absorbed in the reactor by the gas mixture is a factor that largely determines the mechanical characteristics of the synthesized material. In turn, the absorbed energy is determined by linear velocity of the gas flow and temperature. These two parameters allow controlling the output of the material keeping or changing balance between them. To increase the yield of material, it is necessary to increase both the flow rates of gases and the temperature.

It should be noted that the quality of the material is also affected by the laminarity of the gas flow in the near-surface region, which is mainly dictated by the geometry of the reactor zone. Gas flow control in our set-up is realized using stable gas flow regulators and maintaining a uniform pumping speed. For this reason, controlling the synthesis temperature and maintaining its stability is of paramount importance in the synthesis process. This is due to the fact that at such high temperatures and electric current values the structural inhomogeneities of the graphite assembly and the heating element affect temperature distribution over the deposition zone, which begin to heat up inhomogeneously. We expect that this effect might be diminished by applying a high-frequency heating current. However, this requires more detailed study and will be done in the future.

In the synthesized material, the boron concentration was maintained at the level of 15–19 at.%, similar to that reported in Refs. [9,31]. We restricted ourselves to this concentration range taking into account the conclusion made in [29] that B_xC_{1-x} materials with a high boron content (more than 20 at.%) have ultrahigh hardness, but are also very brittle, which limits their practical use. One factor to consider is the different reaction rates for the decomposition of hydrocarbons and boron trichloride. The latter reaction is slower and, correspondingly, the boron concentration along the sample changes upwards. Therefore, the samples obtained in one synthesis have a gradient of boron concentration and, consequently, mechanical characteristics. In our synthesis we selected the conditions in such a way that the output of the material with the required mechanical characteristics was maximal.

Concluding this subsection, in Table 1 we present generalized collection of main properties of the material synthesized in our CVD set up. The variation of the properties is associated both with the boron content in the gas mixture and synthesis temperature as well as with the samples position on the vertical axis along the movement of the mixture. In the next section we will study this issue in more detail.

2.2. Samples preparation

As mentioned above, as a result of synthesis, a hexagonal prism is formed, which is cut into six rectangular plates. The synthesis time depends on the required thickness of the resulting material. The duration of the synthesis of the samples described in the article (2.5–3 mm) is about 6 h. Then one of the plates was divided into three parts and S_t, S_m and S_b samples, were taken from the upper, middle and lower partы, respectively. The general view is shown in picture Fig. 2. The sawn sections were polished and then used for research. Polishing was carried out using standard polishing equipment for sample preparation on a rotating disk, using clean water to clean the abrasive disks. To assess the surface quality, the roughness R_a was measured using a TIME 3221 roughness meter on a 2.5 mm track: $R_a = 0.10$ μm for S_t sample, and $R_a = 0.12$ μm for S_m and S_b samples. We associate the differences in the quality of processing with a higher concentration of boron carbide agglomerates in samples from the middle and bottom of the reactor, which have greater hardness compared to pyrolytic carbon and, accordingly, are less polished under the same conditions.

Table 1
Properties of the synthesized B-PyC.

Physical characteristic	Value
Density, g/cm^3	1.8–2.1
Microhardness, HV	60–200
Modulus of elasticity, GPa	20–25
Bending strength, MPa	250–450
Boron content, at.%	4–19
Electrical properties	To be delivered elsewhere

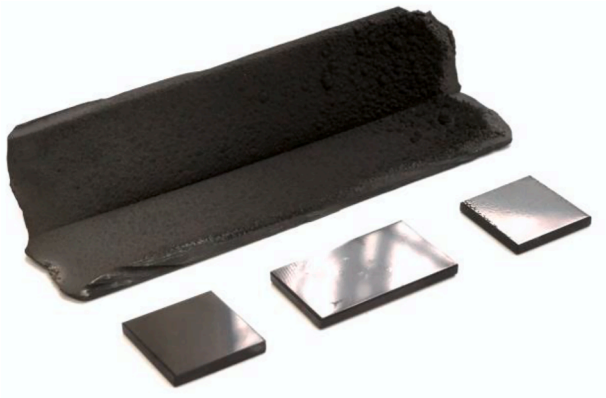

Fig. 2. Photo of two uncut plates from the synthesized prism and polished samples extracted from three different parts of a plate: top, middle and bottom. The length of the plates is about 100 mm.

2.3. Microstructural analysis

Fig. 3 shows scanning electron microscopy images (SEMS-4800 Hitachi) of B-PyC samples synthesized as a result of the deposition reaction along the top-down flow of input reactive gases inside the hexagonal prism reaction zone. All three samples demonstrate a well-developed surface, characteristic of the conditions of pyrolytic synthesis, in which the growth of curved lamellas of a graphite-like phase is observed [12,32]. These lamellas are compositions of thin graphite/graphene layers, randomly stacked on top of each other and highly entangled, with a rather low degree of crystallinity. The boron carbide particles are embedded in the pyrolytic carbon phase so that the lamellae bend around them. The distances between atomic planes in pyrolytic carbon lamellae are estimated to be in the range of 0.3428–0.3443 nm [2]. Such structural features provide isotropy of the material characteristics and excellent mechanical properties of the material. As one can see, a homogeneous and fairly dense material with a small number of micropores is deposited in the upper part of the reaction zone (Fig. 3a). For samples located deeper in the chamber (see Fig. 3b,c), a slight decrease in the size of the lamellas is observed, which is especially noticeable for the sample extracted from the bottom part of the reactor, Fig. 3c. This sample demonstrates a fine-grained structure with more spherical grains.

The images show that during the formation of an isotropic carbon phase in B-PyC, pores are formed with an average size of 2–10 μm. Analogous effect was reported in [27] for pyrolytic carbon. The pores are evenly distributed over the material growth plane. It can be seen that all samples have a well-developed surface formed by curved lamellae of a graphite-like phase. This structure is characteristic of pyrolytic synthesis processes. [1]. We also note a decrease in the size of the structural elements of the surface as we move from top to bottom of the reactor zone.

As a result of studying the temperature dependences of the structure of the material, we came to the conclusion that at low temperatures, the formation of large graphite lamellae is observed in the microstructure of the material, which reduce the hardness of the material. The role of this effect decreases with increasing synthesis temperature. We used this property when choosing the temperature in the reactor.

X-ray phase analysis of the samples was carried out in parallel beam

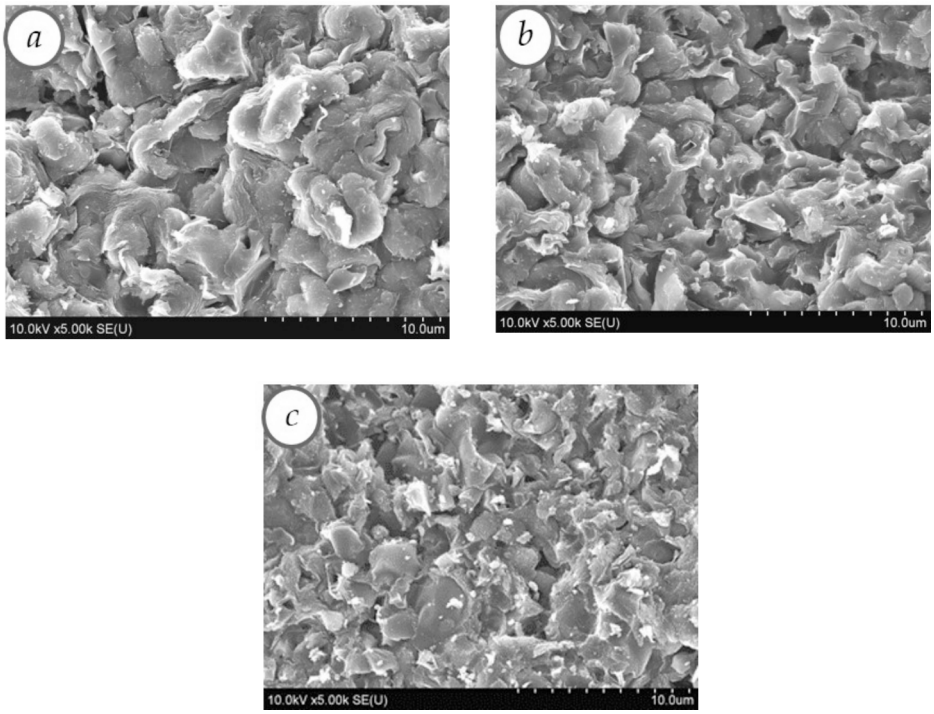

Fig. 3. Scanning electron microscopy of samples extracted from the different places of B-PyC plate: (*a*) from the top (S_t) containing 92.56 wt% of carbon, 3.96 wt% of boron and 3.48 wt% of oxygen; (*b*) from the middle part (S_m) in which the content of carbon, boron and oxygen is 84.06 wt%, 15.09 wt%, and 0.86 wt%, respectively; (*c*) from the bottom part (S_b) with 81.05 wt% of carbon, 18.29 wt% of boron and 0.66 wt% of oxygen.

geometry on a Rigaku ULTIMA IV diffractometer with the copper cathode (radiation wavelength of 0.15418 nm). The X-ray diffraction pattern of samples was fixed in the angle range $2\theta = 10$–100 grad with a step of 0.05 grad and a detector speed of 2 grad/min. Fig. 4 shows the phase composition of studied samples *a-c* from Fig. 3. The figure demonstrates formation of a two-phase system in all samples consisting of pyrolytic graphite (spatial lattice – hexagonal P63/mmc) and boron carbide B_4C (hexagonal lattice R-3m lattice). The boron content in the structure, extracted from the electron microscopy, correlates well with the intensities of the peaks corresponding to the B_4C phase in the X-ray spectra.

The difference observed in the structure over the reactor zone can be understood assuming that the structure is mainly depends on the thermal energy absorbed by the gas mixture during its movement along the reaction zone. In the upper part the energy absorbed by boron trichloride is quite small to provide its full decomposition. As a result, pyrolytic carbon with a low boron content is formed. In the lower part of the reactor, the supply of thermal energy is sufficient to ensure complete decomposition of boron trichloride and form a finer grained structure. Thus, with increasing boron concentration, a transition from flake-like structure to fine-grained-spherical microstructure is observed. This allows us to assume that boron is a nucleating agent for the deposition of

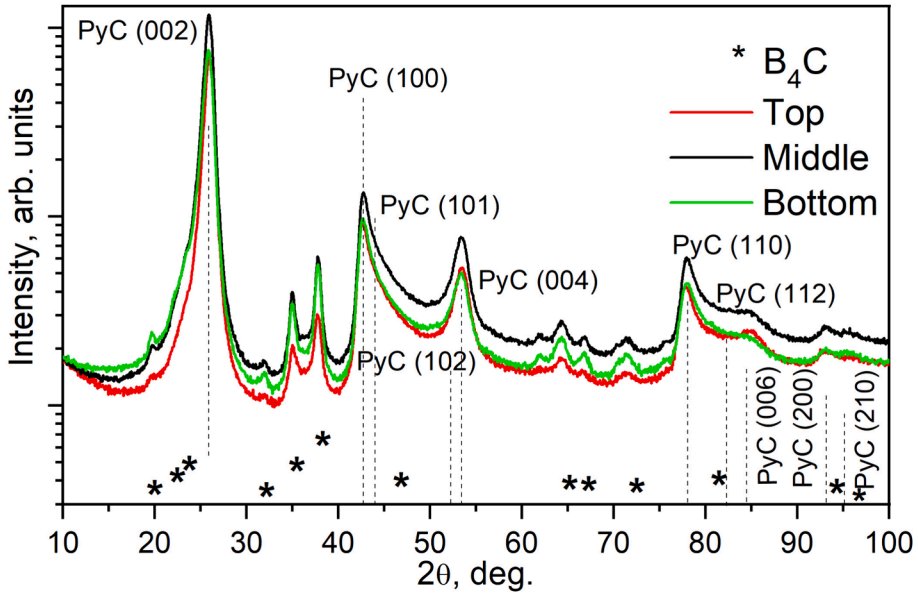

Fig. 4. Phase composition of the samples a,b,c from Fig. 2. The symbol * marks the B_4C phase.

pyrolytic carbon with the formation of carbides, which act as the nuclei of microcrystallite agglomerates. Lattice parameters of pyrolytic carbon and boron carbide B_4C in the structure of samples from three different parts of reactor zone are presented in Table 2.

To confirm the mechanisms of formation of boron-doped pyrolytic carbon material, transmission electron microscopy (TEM) images of the structure were taken. A sample located in the middle of the reactor (S_m) was studied. The density of crystallites packing in a macrovolume depends on the variation in the technological conditions of deposition and location in the reactor zone. TEM micrographs were obtained with Themis-Z 3.1 instrument (TFS, USA) equipped with X-FEG-monochromator and CS/S double corrector, accelerating voltage 200 kV. Elemental analysis was performed with Super-X EDS detector (energy resolution about 120 eV) in HAADF-STEM mode. The samples for the TEM study were prepared by ultrasonic dispersing in ethanol and consequent deposition of the suspension upon a "holey" carbon film supported on a copper grid.

Fig. 5a shows that boron atoms (red color) are unevenly distributed throughout the surface in the form of fairly large clusters. This confirms the formation of B_4C microcrystallites in the pyrolytic carbon matrix, which in turn act as nucleators for formation of larger agglomerates responsible for the increased strength of the material. These results are in good qualitative agreement with the principles of formation of the structure of pyrolytic carbon [1]. Region 1 from Fig. 5a, shown in enlarged form in Fig. 5b, is characterized by a parallel arrangement of graphite layers. Fig. 5c represents region 2 from Fig. 5a, which is characterized by a high concentration of boron atoms. In contrast to region 1, in region 2 the material consists of intertwined layers of graphite due to formation of B_4C microcrystallites.

Fig. 5d demonstrates growth of a triangle regions of B-PyC on the substrate surface. As the synthesis proceeds, the B-PyC regions slowly expand and fill the entire surface of the substrate and then form a bulk material. Inside the triangle, sheets of carbon atoms form a graphite-like layered structure. Although we see a triangle-like object on Fig. 5d, we assume that in the general case the shape of the growth region can be arbitrary with boron atoms as nuclei.

Based on the data presented, we can conclude that as a result of high-temperature pyrolysis of a mixture of reaction gases – methane, propane, boron trichloride and nitrogen, added to maintain optimal absolute pressure – a two-phase system is formed in the reactor, consisting of intertwined graphite sheets surrounding microcrystallites of boron carbide, evenly distributed throughout the volume of material. As a result, this material exhibits the effect of combining the properties of high hardness of boron carbide with high strength of carbon bonds. The presence of a sufficiently high number of structural defects in the material leads to high plasticity of the material compared to crystalline boron carbide while maintaining high mechanical strength and wear resistance.

2.4. Microhardness measurements

In the process of studying the mechanical characteristics of the syntesized material, it was found that it has the property of restoring the surface at low values of mechanical loads, that is, it is elastic under such loads. Microhardness measurements were carried out using the Vickers method with the application of a thin intermediate layer with a high plasticity (see Fig. 6).

As can be seen from the figure, the use of such a layer makes it possible to measure the diagonal of the indentation and thus determine the microhardness under conditions of elastic deformation of the material. Sprayed films of metals with a thickness less 50 nm or other coatings that leave a visible mark can act as an intermediate layer. We used thin wax layer. The study was carried out on a Wilson Instruments 402MVD hardness tester with an indenter load of 50 g and holding time 30 s. The measurements performed gave a value of 60–80 HV for samples from the top part of the reactor zone, 90–110 HV for the middle and 160–200 HV for the bottom. Note that the results obtained were previously presented in summary Table 1. Since the boron content in the material increases as the gas mixture moves in the reactor, we can state that an increase in boron concentration leads to an increase in microhardness. This is related to the two phase structure of the synthesized material. One of them is formed by hard BC_4 agglomerates and thus provides the effect.

The macroscopic hardness of the samples was determined by the Rockwell method (AFRI-URBV-VRS, Italy) with a load of 150 kgf on a diamond indenter with a radius of curvature of 200 μm. Studies have shown that, in contrast to microhardness, hardness values for all samples are comparable, demonstrating a gradual decrease as one moves deeper into the reactor zone: HRC 65.5, 62.6 and 56.3 for S_t, S_m and S_b samples, respectively. This difference in the behavior of hardness is due to the fact that microhardness was measured well within the elastic limit of the material, while macroscopic hardness was measured under loads significantly exceeding this limit.

2.5. Tribological testing

The study of tribological characteristics was carried out on an automated tribometer operating according to the "ball-disk" test scheme. A steel ball with a diameter of 5.5 mm and a hardness of 63 HRC was used as a counterbody. The load on the sample was 2 N, the disk rotation speed was 80 rpm. The device allows measuring the friction coefficient with an accuracy of 0.01. The diameter of the friction track is 13 mm. For all three samples, the test time was about 2 h. After testing each of the samples, photographs of the friction track, as well as the contact spot of the counterbody, were taken using an optical microscope with a magnification of 10× and 20×. The friction track profile measurements were carried out using a profilometer Mitutoyo Surftest SV-2100, Japan, at a load 0.75 mN, an angle of the measuring tip of 60 grad, and a radius of the measuring tip of 2 μm. The dependence of the friction coefficient μ on test time for samples S_t, S_m, and S_b, located at the top, middle and bottom of the reactor, respectively, is shown in Fig. 7.

For the obtained samples of boron-enriched pyrolytic carbon, the friction coefficient values are in the range of 0.10–0.16. It should be noted that pyrolytic carbon obtained under similar conditions in Ref. [32], but without introducing boron-containing gases into the reactor, has similar friction coefficient at the level of 0.14–0.16. At the same time, Refs. [35,36] report the positive effect of boron carbide and nitride phases on the tribological properties of carbon materials. In terms of the friction coefficients, the resulting pyrolytic carbon material is comparable to diamond-like carbon, which has record low friction coefficients [37].

The S_b and S_m samples demonstrate high stability of the friction coefficient. Its change during two-hour tests after a short running-in period is only a few percent. A significant difference in the dynamics of friction is observed for sample S_t, which contains the least amount of boron. The graph μ(t) is very "noisy" (see Fig. 7): the value of the friction coefficient in a short time interval changes abruptly within a few hundredths. It is characterized by a significantly longer running-in period, which is about 10 min, after which μ stabilizes at the level of 0.16. After approximately 50 min of testing, a smooth decrease in the friction force occurs, and the friction coefficient stabilizes over time at 0.11,

Table 2
Lattice parameters of PyC and B_4C in the in the structure of samples from different parts of the reactor zone.

Position in the reactor	Lattice parameters of PyC, nm		Lattice parameters of B_4C, nm	
	a, b	c	a, b	c
S_t	2,440	6,880	5,579	12,050
S_m	2,450	6,863	5,558	12,100
S_b	2,449	6,850	5,643	12,094

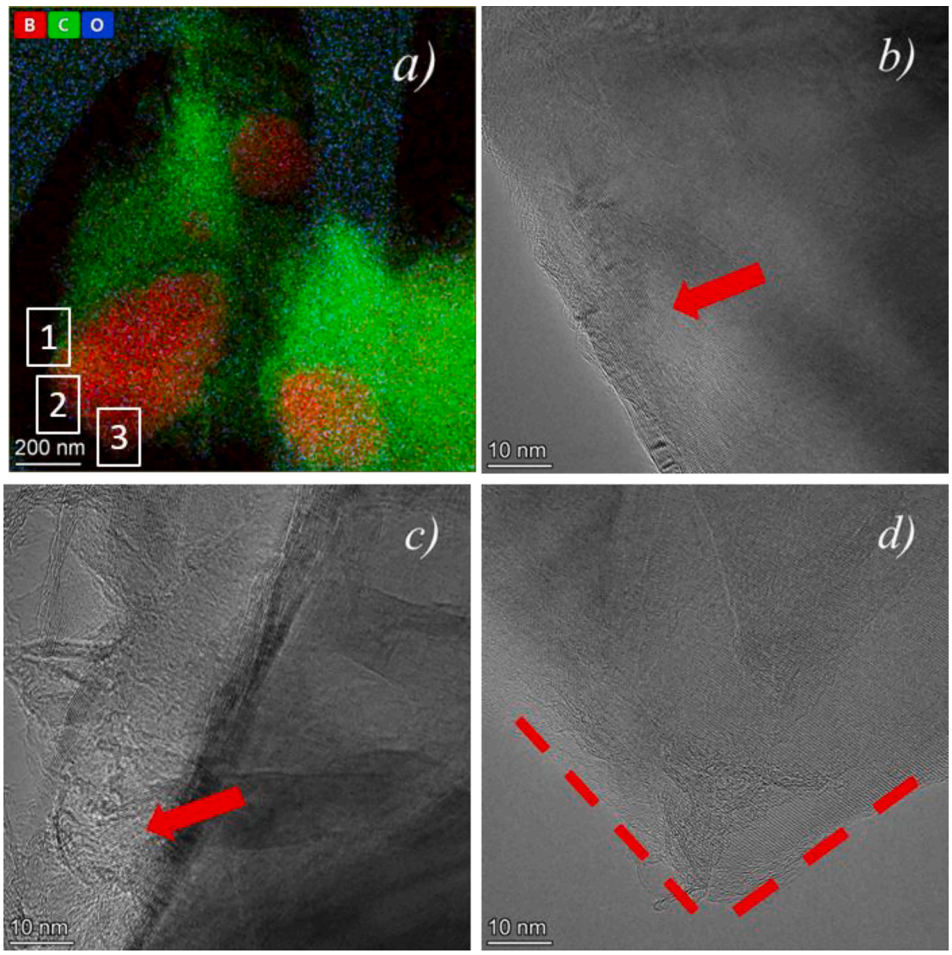

Fig. 5. Energy dispersive X-ray (EDX) mapping (*a*), and high resolution TEM images of regions 1–3 from picture (*a)* are marked by indices (*b)-(d),* respectively. Distribution of boron, carbon and oxygen atoms are given in picture (*a*) in red, green and blue colors.

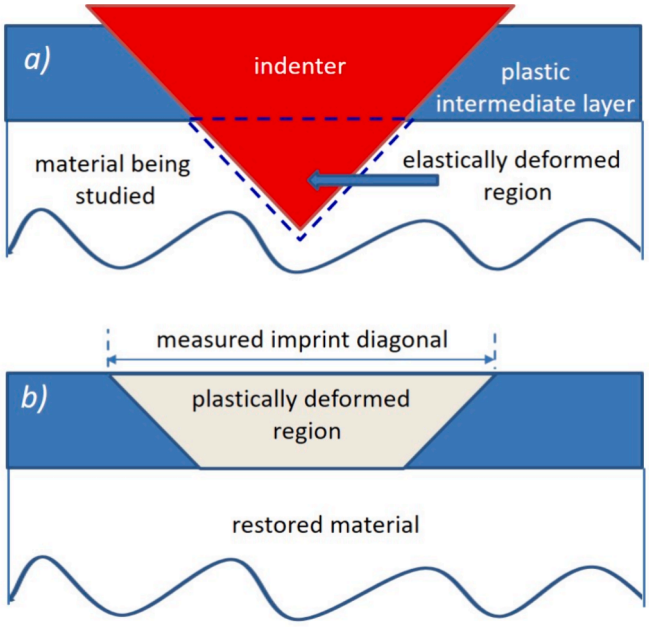

Fig. 6. Schematics of the measuring procedure under condition of the elastic deformation of the studied material.

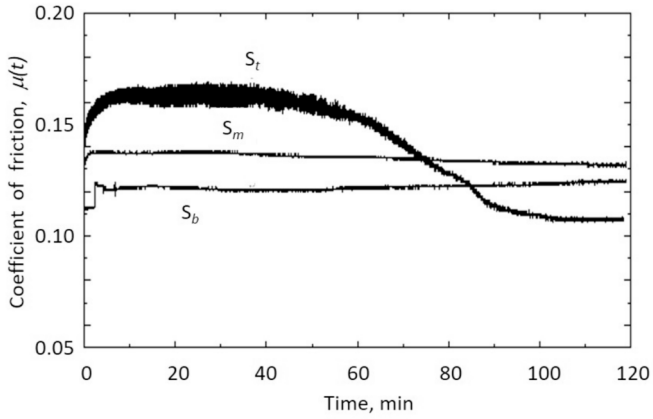

Fig. 7. Change in the dry friction coefficient during tribological tests of samples S_t, S_m, and S_b.

accompanied by a decrease in the spread of values. Fig. 7 is the lowest for the entire series of samples. In this case, there is a tendency for the values of the friction coefficients to converge for all three samples during a long process.

We associate this behavior of the friction coefficient for a sample with a lower boron content with the effect of running-in of the rubbing surfaces at the initial time. In this case, the carbon formed as a result of friction has a lubricating effect, which leads to a significant drop in the

friction coefficient. For samples with a higher boron concentration, this effect is practically absent, since the sediments formed as a result of friction contain much more boron carbide, which does not provide a lubrication effect.

Fig. 8, using sample S_t as an example, shows a friction track characteristic of all three samples (light area highlighted by dashed lines). It can be seen that the friction path is smoother compared to the surrounding areas, and there is little material removal from it due to the low coefficient of friction, despite the long tribological test time. As is known, the tribological characteristics of a material for dry friction conditions are strongly influenced by its hardness [33], as well as surface morphology [34]. The latter is especially important for the friction of hard materials with a relatively soft counter-body. High surface roughness leads to severe abrasive wear of the counter-body. This kind of strong interaction between rubbing surfaces leads to an increase in the friction force and, accordingly, the friction coefficient. In this case, the time of lapping-in and formation of the tribological layer increases with increasing macrohardness. At the same time, hard materials with high surface smoothness, as a rule, have lower friction coefficients.

Based on these data, it is possible to explain the initially low values of the friction coefficient for the S_b and S_m samples compared to the S_t one. Over time, the grinding in rubbing surfaces reduces for sample S_t the effect of roughness and, as a result, the friction coefficient decreases quickly. In the case of S_b and S_m samples we observe only a small variation of the friction coefficient. This is because the microhardness of these samples is much high (see Sect 2.4) due to increasing presence of B_4C agglomerates in the microstructure. From a comparison of the width of the friction tracks, it follows that the widest track, 166 μm, is for sample S_t due to severe wear of the steel ball and an increase in the area of its contact with the surface of the sample. The presence of hard flakes in the microstructure also affects the appearance of "noise" in the friction curve (Fig. 7). As the friction process progresses, rubbing surfaces the rubbing surfaces are run-in and the noise decreases.

The wear mechanism described is confirmed by analysis of the surface of the tribological layer on the counter-body surface. A SEM photograph of a fragment of the contact spot of a steel ball for sample S_t is shown in Fig. 9. This fragment contains a fairly thick layer of carbon material (Area 1 in Fig. 9), formed as a result of friction in the contact zone. Its elemental composition, as well as the elemental composition of the neighboring regions in the non-contact area (Area 2) and the dendritic particle (Area 3), is given in Table 3. In addition to carbon, the sediment layer contains a large amount of oxygen. The presence of oxygen is due to graphitization of the material as a result of friction.

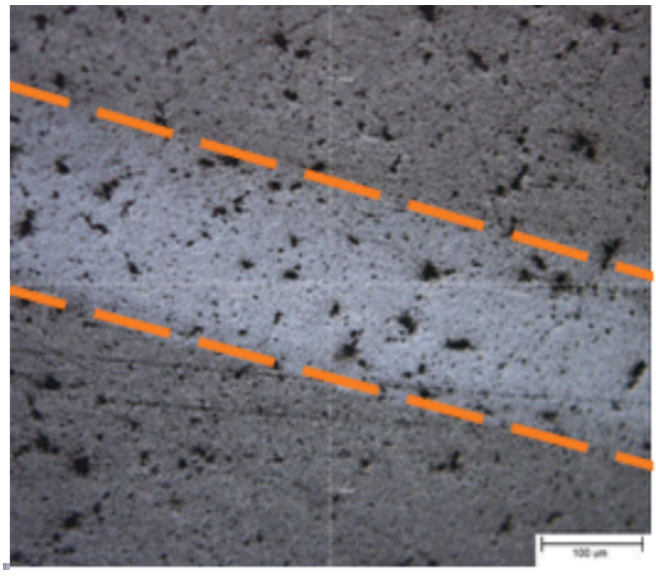

Fig. 8. Optical photograph of a fragment of the friction track (highlighted by dashed lines) for sample S_t.

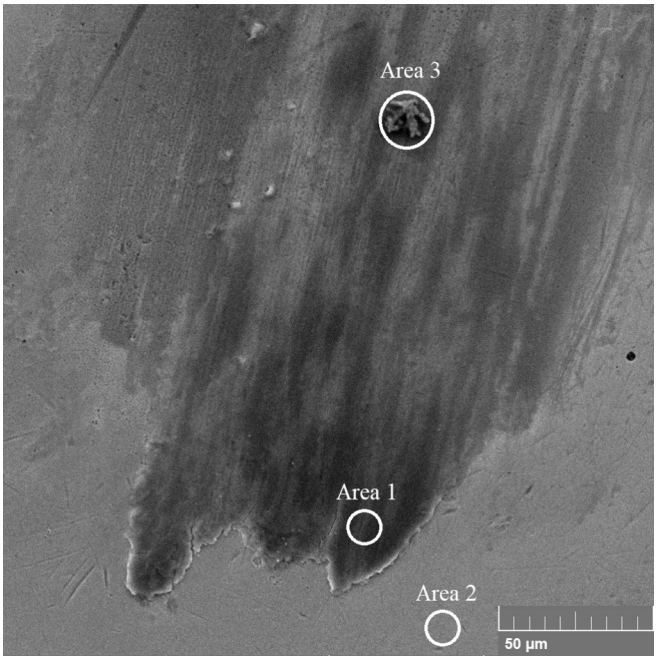

Fig. 9. SEM photograph of the contact spot on the counter-body surface with a B-PyC tribological layer on the counterbody surface (EDX analysis areas are highlighted).

Table 3
Elemental composition of various fragments of the contact spot of the contact body (at. %).

Chemical elements	Area 1	Area 2	Area 3
B	4.6	0	31.3
C	35.9	20.4	41.6
O	34.6	0.3	0
Chemical elements of the steel ball			
Cr	0.5	1.4	0.8
Mn	0	0.2	0.1
Fe	24.4	77.6	26.1

2.6. Formation of dendrite-like structures

If a small amount of oxygen-containing compounds (from 0.01 to 2 vol%) are added to the reaction chamber, such as water vapor or atmospheric air, the layer-by-layer growth of the material is disrupted and tree-like dendritic structures are formed. Fig. 10 shows an example of the obtained samples. In this case, there is a significant decrease in the yield of dense isotropic material suitable for further mechanical processing. Note that the resulting columnar structure may be of particular interest for biomedical and electrochemical applications as a basis for electrodes with a large contact area. Elucidation of the features of the mechanisms of columnar structure formation requires more detailed research. Early reports on the formation of a spherically symmetrical ball structure of pyrolytic carbon are given in Ref. [38].

The formation of dendrites is associated with a violation of the symmetry of the boron–carbon material, which is caused by the replacement of carbon atoms with oxygen atoms. Possible bonding structures of boron atom in CVD boron-doped carbon has been presented in Ref. [23, Fig. 8]. The replacement of carbon with oxygen atoms leads to the breaking of bonds and prevents the growth of the material. When the oxygen concentration increases to more than 3–4 vol%, the growth

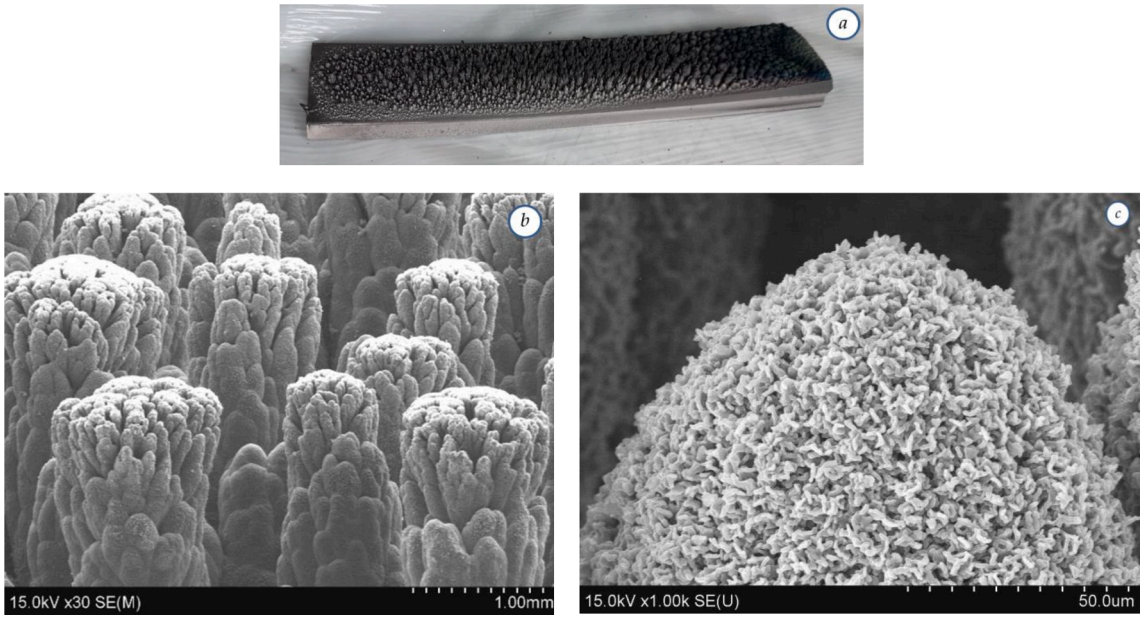

Fig. 10. Columnar structure on the surface of the substrate, formed when oxygen-containing gases are added at a temperature of 1570 °C. General view of the plate with B-PyC on the graphite substrate (*a*) and columnar structure at different magnification (*b,c*). The content of boron, carbon and oxygen in columnar objects depicted is 9.09, 89.57 and 1.34 wt%, respectively.

rate of the material on the plates in the reactor decreases significantly. The material is deposited in the form of a fine-grained soot fraction in the filter element.

2.7. Oxidation resistance

In an inert environment or in a vacuum, pyrolytic carbon material remains functional up to 2500–2800 °C. However, in an oxidizing environment, intense pyrolytic carbon oxidation begins already at temperatures above ~700 °C [39]. Therefore, one of the main tasks that determines the performance of structures at high temperatures is the development of protective anti-oxidation coatings. To protect carbon–carbon materials at temperatures up to 1500–1650 °C, volumetric protection methods are applied to carbon matrix [40]. However, the use of materials with different coefficients of thermal expansion leads to an increase in internal stresses during thermal cycling. Therefore, it is of great interest to study the behavior of uncoated pyrolytic carbon material when heated. Thermogravimetric analysis (TGA) and differential thermal analysis (DTA) were carried out on a NETZSCH STA 449 F3 Jupiter synchronous analyzer in air as oxidizing environment, with heating rate 10 K/min, Al_2O_3 crucibles, and 17 mg samples made of graphite and S_m B-PyC. The results are shown at Fig. 11.

In Fig. 11a one can see that the heating curves of samples of graphite and pyrolytic carbon practically coincide up to a temperature of 700–750 °C, while heated to higher temperatures, graphite begins to oxidize with a significant decrease in mass and with the release of heat (Fig. 11b). A slight excess of the samples weight over 100 % (Fig. 11a) is associated with the technical features of the device and does not affect the nature of the identified dependencies. Unlike graphite, pyrolytic carbon practically does not lose mass over the entire range of measured temperatures, up to 1200 °C, see Fig. 11a. This indicates the high heat resistance of the resulting material. Note also that the DTA curve is smooth and can be approximated by a straight line with minor deviations. This indicates the absence of phase transitions in the measured temperature range. Thus, it can be argued that in the given temperature range, boron-enriched pyrolytic carbon is thermostable.

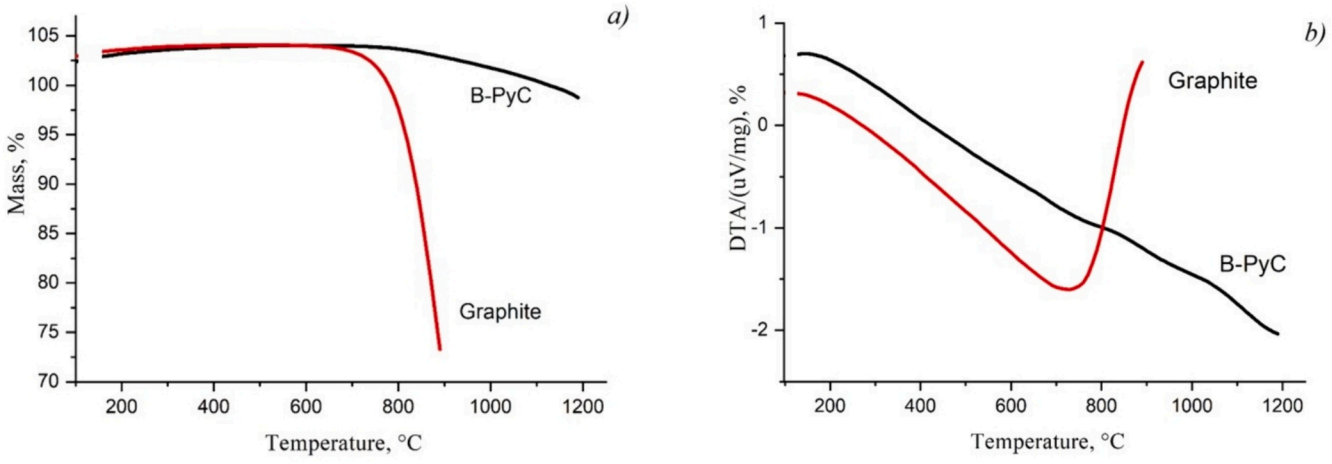

Fig. 11. Comparative thermogravimetric analysis of B-PyC and graphite samples: *a)* TGA, *b)* DTA.

3. Summary and outlook

In the paper, we demonstrated a new realization of the traditional CVD method for the synthesis of boron-enriched pyrolytic carbon (B-PyC) material. The synthesis occurs in a vertically oriented reactor zone from a boron trichloride/methane/propane/nitrogen gaseous reaction mixture. The vertical orientation of the reactor provides, on the one hand, the possibility of synthesizing material in macroscopic quantities, and on the other hand, leads to variations in material parameters along the reactor zone. Depending on the potential applications, such variability may either reduce the useful yield of the material or not have a significant impact. In any case, this problem exists and a technological solution should be found in the future.

As it has been shown, the microhardness of the synthesized material is varied in the range of 60–200 HV, dependently on the boron content and sample position in the reactor zone. Attractive for applications are its mechanical and tribological characteristics, which are determined by the concentration of bound boron in the material. Tribological and elastic properties of the material (modulus of elasticity ~20–25 GPa and bending strength ~250–450 MPa) and its low density, allow, in addition to medical applications in traumatology and cardiac surgery, its use in metallurgy, aircraft manufacturing and rocketry. In these same tasks, an important property of the material is its heat resistance: The material demonstrates high heat resistance and high thermal stability in air at least up to a temperature of 1200 °C, which significantly exceeds these characteristics for graphite and pyrolytic carbon without incorporated boron. Also we consider boron–carbon dendritic structures (Fig. 10) interesting and promising for applications in electrochemistry and bioengineering.

CRediT authorship contribution statement

Marina Demidenko: Methodology, Investigation, Conceptualization. **Dzmitry Adamchuk:** Writing – original draft, Methodology, Investigation. **Alexander Liubimau:** Visualization, Resources, Investigation. **Vladimir Uglov:** Visualization, Resources, Investigation. **Arcady Ishchenko:** Visualization, Resources, Investigation. **Mikalai Chekan:** Visualization, Resources, Investigation. **Mikhail Khama:** Visualization, Resources, Investigation. **Sergey Maksimenko:** Writing – review & editing, Supervision, Conceptualization.

Declaration of competing interest

The authors declare that they have no known competing financial interests or personal relationships that could have appeared to influence the work reported in this paper.

Data availability

Data will be made available on request.

Acknowledgement

Authors acknowledge a support from the plant “ELECTRONMASH”, Minsk, Belarus. Transmission electron microscopy investigation was supported by project FWUR-2024-0032, Russia. The scanning electron microscopy has been carried out at the State Center “Belmicroanalysis” of JSC “INTEGRAL”, Minsk, Belarus.

References

[1] J.C. Bokros, Deposition, Structure and Properties of Pyrolytic Carbon, in: P.L. Walker (Ed.), Chemistry and Physics of Carbon, vol. 4, Marcel Dekker, Inc., New York, 1969, pp. 1–118.
[2] R.B. More, A.D. Haubold, J.C. Bokros, Pyrolytic Carbon for Long-Term Medical Implants, in: B.D. Ratner (Ed.), Biomaterials science: an introduction to materials in medicine (third edition), Academic Press, 2013, pp. 209–222, https://doi.org/10.1016/B978-0-08-087780-8.00023-1.
[3] G. Serino, M. Gusmini, A.L. Audenino, G. Bergamasco, O. Ieropoli, C. Bignardi, Multiscale characterization of Isotropic pyrolytic carbon used for mechanical heart valve production, Processes 9 (2021) e338, https://doi.org/10.3390/pr9020338.
[4] G.P. Keeley, N. McEvoy, S. Kumar, N. Peltekis, M. Mausser, G.S. Duesberg, Thin film pyrolytic carbon electrodes: a new class of carbon electrode for electroanalytical sensing applications, Electrochem. Commun. 12 (2010) 1034–1036, https://doi.org/10.1016/j.elecom.2010.05.017.
[5] J.F.S. Pereira, R.G. Rocha, S.V.F. Castro, A.F. Joao, P.H.S. Borges, D.P. Rocha, A. Siervo, E.M. Richter, E. Nossol, R.V. Gelamo, R.A.A. Munoz, Reactive oxygen plasma treatment of 3D-printed carbon electrodes towards high-performance electrochemical sensors, Sens. Actuators B Chem. 347 (2021) 130651, https://doi.org/10.1016/j.snb.2021.130651.
[6] M.M. Li, X. Fan, W.T. Zheng, First-principle calculations on the structural stability and electronic properties of superhard B_xC_y compounds, J. Phys. Condens. Matter. 25 (2013) e425502, https://doi.org/10.1088/0953-8984/25/42/425502.
[7] C.E. Lowell, Solid solution of boron in graphite, J. Am. Ceram. Soc. 50 (1967) 142–144, https://doi.org/10.1111/j.1151-2916.1967.tb15064.x.
[8] S. Marinković, Č. Sužnjević, I. Dežarov, Simultaneous pyrolytic deposition of carbon and boron, Carbon 7 (1969) 185–193, https://doi.org/10.1016/0008-6223(69)90016-5.
[9] B.M. Way, J.R. Dahn, T. Tiedje, K. Myrtle, M. Kasrai, Preparation and characterization of B_xC_{1-x} thin films with the graphite structure, Phys. Rev. B 46 (1992) 1697–1702, https://doi.org/10.1103/physrevb.46.1697.
[10] D.L. Fecko, L.E. Jones, P.A. Thrower, The formation and oxidation of BC_3, a new graphite-like material, Carbon 31 (1993) 637–644, https://doi.org/10.1016/0008-6223(93)90119-U.
[11] R. Hu, T.C. Chung, Synthesis and characterization of novel B/C materials prepared by 9-chloroborafluorene precursor, Carbon 34 (1996) 1181–1190, https://doi.org/10.1016/0008-6223(96)00064-4.
[12] Xu. Li, Wu. Junfeng, S. Bai, Fabrication and microstructure of boron-doped isotropic pyrolytic carbon, Carbon 50 (2012) 4705–4710, https://doi.org/10.1016/j.carbon.2012.05.062.
[13] I. Annuar, J. Rouhi, M. Ruso, Boron-doped amorphous carbon film grown by bias assisted pyrolysis chemical vapor deposition, IEICE Electronics Express. 12 (2015) 1–10, https://doi.org/10.1587/elex.11.20140937.
[14] N.P. Stadie, E. Billeter, L. Piveteau, K.V. Kravchyk, M. Döbeli, M.V. Kovalenko, Direct synthesis of bulk boron-doped graphitic carbon, Chem. Mater. 29 (2017) 3211–3218, https://doi.org/10.1021/acs.chemmater.7b00376.
[15] M. Chasmawala, T.C. Chung, Synthesis of B/C materials from boron-containing phenyl acetylides, Carbon 35 (1997) 641–650, https://doi.org/10.1016/S0008-6223(97)00019-5.
[16] Q. Hu, Q. Wu, Y. Ma, L. Zhang, Z. Liu, J. He, H. Sun, H.-T. Wang, Y. Tian, First-principles studies of structural and electronic properties of hexagonal BC_5, Phys. Rev. B 73 (2006) e214116, https://doi.org/10.1103/PhysRevB.73.214116.
[17] P.A. Baker, S.A. Catledge, S.B. Harris, K.J. Ham, W.-C. Chen, C.-C. Chen, Y. K. Vohra, Computational predictions and microwave plasma synthesis of superhard boron-carbon materials, Materials 11 (2018) e1279, https://doi.org/10.3390/ma11081279.
[18] J.Y. Howe, L.E. Jones, Influence of boron on structure and oxidation behavior of graphite fiber, Carbon 42 (2004) 461–467, https://doi.org/10.1016/j.carbon.2003.09.023.
[19] X. Wu, L.R. Radovic, Inhibition of catalytic oxidation of carbon/carbon composites by boron-doping, Carbon 43 (2005) 1768–1777, https://doi.org/10.1016/j.carbon.2005.02.029.
[20] Q. Tong, J. Shi, Y. Song, Q. Guo, L. Liu, The influences of boron on strength and ablation resistance of zirconium-doped graphitised carbons, Carbon 43 (2005) 2013–2015, https://doi.org/10.1016/j.carbon.2005.01.038.
[21] A. Becker, J. Gremmels, K.J. Hüttinger, Sintering of powders of polyaromatic mesophase to high-strength isotropic carbon-IV powders based on boron-substituted mesophase, Carbon 37 (1999) 953–960, https://doi.org/10.1016/S0008-6223(98)00250-4.
[22] A. Agrawal, H. Yinnon, D.R. Uhlmann, R.T. Pepper, C.R. Desper, Boron modification of carbon fibres, J. Mater. Sci. 21 (1986) 3455–3466, https://doi.org/10.1007/BF02402987.
[23] Y. Liu, L. Zhang, L. Cheng, W. Yang, Y. Xu, Effect of deposition temperature on boron-doped carbon coatings deposited from a BCl_3–C_3H_6–H_2 mixture using low pressure chemical vapor deposition, Appl. Surf. Sci. 255 (2009) 8761–8768, https://doi.org/10.1016/j.apsusc.2009.06.030.
[24] S. Ha, G.B. Choi, S. Hong, D.W. Kim, Y.A. Kim, Substitutional boron doping of carbon materials, Carbon Lett. 27 (2018) 1–11, https://doi.org/10.5714/CL.2018.27.001.
[25] F. Ali, N.S. Hosmane, Y. Zhu, Boron chemistry for medical applications, Molecules 25 (2020) 828, https://doi.org/10.3390/molecules25040828.
[26] F. Liu, X. Zhao, P. Shi, L. Li, Q. Dong, M. Tian, Y. Wu, X. Sun, A review on recent progress achieved in boron carbon nitride nanomaterials for supercapacitor applications, Batteries 9 (2023) e396, https://doi.org/10.3390/batteries9080396.
[27] E. López-Honorato, P.J. Meadows, P. Xiao, Fluidized bed chemical vapor deposition of pyrolytic carbon – I. Effect of deposition conditions on microstructure, Carbon 47 (2009) 396–410, https://doi.org/10.1016/j.carbon.2008.10.023.
[28] T. Shirasaki, A. Derre, M. Menetrier, A. Tressaud, S. Flandrois, Synthesis and characterization of boron-substituted carbons, Carbon 38 (2000) 1461–1467, https://doi.org/10.1016/S0008-6223(99)00279-1.

[29] V. Serin, R. Brydson, A. Scott, Y. Kihn, O. Abidate, B. Maquin, A. Derré, Evidence for the solubility of boron in graphite by electron energy loss spectroscopy, Carbon 38 (2000) 547–554, https://doi.org/10.1016/s0008-6223(99)00128-1.
[30] M.I. Demidenko, D.V. Adamchuk, A.P. Rusanov, S.V. Sirotkin, L.V. Ivanko, S. A. Maksimenko, Boron-enriched pyrolytic carbon: material for biomedical and engineering application, Dokl. Nation. Acad. Sci. Belarus 67 (2023) 250–256, https://doi.org/10.29235/1561-8323-2023-67-3-250-256 (in Russian).
[31] C.T. Hach, L.E. Jones, C. Crossland, P.A. Thrower, An investigation of vapor deposited boron rich carbon–a novel graphite-like material–part I: the structure of BC_x (C_6B) thin films, Carbon 37 (1999) 221–230, https://doi.org/10.1016/s0008-6223(98)00166-3.
[32] Y. Wang, Z. Fan, X. Zhou, C. Zeng, P. Xu, X. Xie, X. Wang, M. Zhang, Z. Su, Q. Huang, Friction properties of bulk isotropic pyrocarbon materials based on different composite microstructures, J. Mater. Res. Technol. 21 (2022) 4079–4092, https://doi.org/10.1016/j.jmrt.2022.11.021.
[33] P. Harlin, C. Per, U. Bexell, M. Olsson, Influence of surface roughness of PVD coatings on tribological performance in sliding contacts, Surface and Coatings Technol. 201 (2006) 4253–4259, https://doi.org/10.1016/j.surfcoat.2006.08.103.
[34] K. Adachi, I.M. Hutchings, Sensitivity of wear rates in the micro-scale abrasion test to test conditions and material hardness, Wear 258 (2005) 318–321, https://doi.org/10.1016/j.wear.2004.02.016.
[35] F. Liu, M. Yi, L. Ran, Y. Ge, K. Peng, Influence of preparation method on microstructure and tribological behavior of C/C-BN composites, Ceramics Intern. 47 (2021) 12879–12896, https://doi.org/10.1016/j.ceramint.2021.01.151.
[36] B. Zhang, P. Xiao, Y. Li, Z. Li, W. Zhou, H. Luo, Y. Lu, Microstructures and tribological properties of carbon/carbon-boron nitride composites fabricated by powdered additives and chemical vapor infiltration, Ceramics Intern. 43 (2017) 7607–7617, https://doi.org/10.1016/j.ceramint.2017.03.055.
[37] K.A.H. Al Mahmud, M.A. Kalam, H.H. Masjuki, H.M. Mobarak, N.W.M. Zulkifli, An updated overview of diamond-like carbon coating in tribology, Critical Rev. Solid State and Mater. Sci. 40 (2015) 90–118, https://doi.org/10.1080/10408436.2014.940441.
[38] A. Raveh, M. Eldan, A. Inspektor, R. Avni, Structure of the solid pyrolysis products produced from propylene in a low-pressure inductive r.f. plasma, Carbon 23 (1985) 179–184, https://doi.org/10.1016/0008-6223(85)90010-7.
[39] V.Z. Shemet, A.P. Pomytkin, V.S. Neshpor, High-temperature oxidation behaviour of carbon materials in air, Carbon 31 (1993) 1–6, https://doi.org/10.1016/0008-6223(93)90148-4.
[40] H. Hatta, R. Weiss, P. David, Carbon/Carbons and their Industrial Applications, in: Ceramic Matrix Composites: Materials, Modeling and Technology, Chapter 5, N.P. Bansal, J. Lamon (Eds.) John Wiley, Hoboken, NJ, 2014, doi: 10.1002/9781118832998.ch5.